Maximizing TADF via Conformational Optimization

Changhae Andrew Kim and Troy Van Voorhis*

Department of Chemistry, Massachusetts Institute of Technology, Cambridge, Massachusetts 02139, United States

E-mail: tvan@mit.edu

Abstract

We investigate a new strategy to enhance thermally activated delayed fluorescence (TADF) in organic light-emitting diodes (OLEDs). Given that the TADF rate of a molecule depends on its conformation, we hypothesize that there exists a conformation that maximizes the TADF rate. In order to test this idea, we use time-dependent density functional theory (TDDFT) to simulate the TADF rates of several TADF emitters, while shifting their geometries towards higher TADF rates in a select subspace of internal coordinates. We find that geometric changes in this subspace can increase the TADF rate up to three orders of magnitude with respect to the minimum energy conformation, and the simulated TADF rate can even be brought into the submicrosecond timescales under the right conditions. Furthermore, the TADF rate enhancement can be maintained with a conformational energy that might be within the reach of modern synthetic chemistry. Analyzing the maximum TADF conformation, we extract a number of structural motifs that might provide a useful handle on the TADF rate of a donor-acceptor (DA) system. The incorporation of conformational engineering into the TADF technology could usher in a new paradigm of OLEDs.

Introduction

Organic light-emitting diodes (OLEDs) are a promising solution in digital displays and lighting applications. Since Tang and Van Slyke demonstrated the first practical OLED device in 1987,[1] OLEDs have attracted widespread research and development (R&D) efforts in both the academia and industry. OLED displays exhibit supremacy in energy efficiency, image quality, response time, and compactness over conventional technologies, such as liquid crystal displays (LCDs).[2–4] In addition, OLEDs are expected to help reduce global energy consumption[5,6] and yield new commercial products, such as transparent lighting panels and flexible displays.[7,8]

A key issue in developing more efficient OLEDs is overcoming the disadvantageous spin statistics. When electrons and holes are injected into the organic layer, they recombine in one of the four possible spin states with equal likelihoods: one singlet state and three triplet states. Whereas the singlet excitons can emit a photon and decay to the likewise singlet ground state, radiative decay of the triplet excitons is spin-forbidden. Most of the exitons are dissipated as heat, and the external quantum efficiency (EQE) of fluorescent OLEDs cannot exceed 25 %. As a way to harvest the triplet excitons, Baldo *et al.* introduced phosphorescent OLEDs (PhOLEDs), which activate the otherwise forbidden transition between the triplet excited state and the singlet ground state.[9] Using the strong spin-orbit coupling (SOC) in heavy metal complexes, the rate of phosphorescence can be brought into the useful microsecond timescale.[7,10] However, in spite of the commercial success of red and green PhOLEDs, an efficient and stable blue PhOLED remains out of reach,[4,11] and the rarity and toxicity of heavy metals are also problematic.

Thermally activated delayed fluorescence (TADF) is an alternative approach of converting the non-emissive triplet excitons to emissive singlet excitons.[12,13] In typical organic molecules, electron exchange stabilizes the first triplet excited state (T_1) with respect to the first singlet excited state (S_1). However, if the singlet-triplet (ST) energy gap is less than few $k_B T$, thermal fluctuations can drive the reverse intersystem crossing (RISC) of the T_1 population

into the S_1 state. Modulation of the exchange energy can be accomplished by tuning the spatial overlap between the highest occupied molecular orbital (HOMO) and the lowerest unoccupied molecular orbital (LUMO). In the first metal-free TADF OLED, Adachi *et al.* employed a donor-acceptor (DA) architecture to localize the HOMO and the LUMO on orthogonal moieties, creating S_1 and T_1 states of charge transfer (CT) character.[14,15] Since then, a large number of TADF emitters have been designed on the same principle,[16–20] and high-throughput screening approaches with the aid of machine learning techniques have been employed to give extensive surveys of the relevant chemical space.[21,22] As a culmination of the R&D efforts, TADF OLEDs are becoming competitive with commercial PhOLEDs.[23–26]

Unfortunately, spatial separation of the HOMO and the LUMO also diminishes the transition dipole moment (TDM) between the S_1 state and the ground state (S_0). A decrease in the TDM entails a decrease in both the prompt and delayed fluorescence rates. The trade-off between a small ST gap and a large TDM is manifest even in the outcomes of high-throughput screening studies.[21,22] In addition, the identical CT character of the S_1 and T_1 states is expected to lead to a vanishing SOC according to El-Sayed's rule[27] and hence a vanishing RISC rate. However, the trade-off might not be an intrinsic limitation of TADF, but an artifact of the design principles based on an oversimplified model. Indeed, recent studies have demosntrated that the T_1 state of many TADF molecules have significant contributions of local excitation (LE)[19,28,29] and that higher triplet states might also have an important role in the RISC step.[28,30,31] The two-state model of TADF does not provide the requisite insight to guide the development of trend-breaking emitters.

Recently, a four-state model of TADF has been proposed that might provide a way to overcome the trade-off.[32] According to the four-state model, the ST gap contains additional terms that can counter the effects of electron exchange, enabling the coexistence of a small ST gap and a large TDM in the same molecule. Furthermore, the adiabatic S_1 and T_1 wavefunctions contain different fractions of diabatic CT and LE wavefunctions, enabling the coexistence of a vanishing ST gap and a non-vanishing SOC. Although the mathematical forms

of the S_1 and T_1 energies and wavefunctions do not render themselves to straight-forward interpretation, exploring the conformation space of TADF emitters has been proposed as a practical approach to discover new design principles. Using molecular dynamics (MD) to sample the conformation space and time-dependent density functional theory (TDDFT) to simulate the electronic excitations, de Silva *et al.* showed that a DA complex can achieve upto an 800-fold enhancement of the TADF rate with respect to the minimum energy conformation.[32] Indeed, a number of theoretical studies have shown that the conformation of a molecule can modulate the excitation energies and state-to-state couplings that contribute to the TADF rate.[33–35] It would be reasonable to believe that the TADF rate has a strong dependence on the conformation.

In this work, we take the idea of conformational dependence to the next step and examine the potential of direct optimization to maximize the TADF rate. Using a number of known TADF emitters, we show that the TADF rate can be enhanced up to three orders of magnitude and can even be brought into the submicrosecond timescales via suitable changes of conformation. The maximum TADF conformation is free of thermal fluctuations that plague MD snapshot geometries, and one can extract specific hints, as well as general principles that can boost the performance of TADF OLEDs. Furthermore, we find that taking a small subset of the conformational variables suffices to gain substantial control over the TADF rate, and the relevant variables seem to overlap with degrees of freedom (DOFs) that might be tunable via steric hindrance or mechanical strain. Hence, conformational optimization appears to herald a new paradigm of TADF OLEDs.

Methods

The TADF rate was estimated using the formulation of Adachi *et al.*[36] First, the rate of TADF is understood to mean the quasi-steady state rate at which the excited states are

depopulated via fluorescence

$$k_{\mathrm{TADF}} \equiv \frac{k_{\mathrm{F}}[\mathrm{S}_1]}{[\mathrm{S}_1] + [\mathrm{T}_1] + [\mathrm{T}_2]} \tag{1}$$

where we have assumed that interal conversion (IC) is fast enough that only the S_1, T_1, and T_2 states have significant populations. In our experience, omission of the T_2 state can lead to an overestimation of the TADF rate when the T_2 energy is below the S_1 energy. Assuming that the forward and reverse intersystem crossing (ISC and RISC) are fast compared to the radiative and non-radiative decay processes, the formula reduces to

$$k_{\mathrm{TADF}} = \frac{k_{\mathrm{F}}}{1 + K_1 + K_2} \tag{2}$$

where K_n is the equilibrium constant between the S_1 state and the T_n state

$$K_n = 3 \exp\left(\frac{\Delta E_{\mathrm{S}_1 - \mathrm{T}_n}}{k_B T}\right) \tag{3}$$

The fluorescence rate is estimated by the Einstein coefficients[37]

$$k_{\mathrm{F}} = \frac{e^2 {\omega_{10}}^2}{2\pi\epsilon_0 m_e c^3} f_{10} \tag{4}$$

where e and m_e are the electron charge and mass, respectively; c is the speed of light; and ω_{10} and f_{10} are the $S_1 \rightarrow S_0$ energy gap and oscillator strength, respectively. In the final objective function, we added a penalty to damp the increase in the conformational energy (the DFT energy with respect to the energy minimum) and byproduct features that might arise in the optimization

$$\Phi = k_{\mathrm{TADF}} - \Lambda \Delta E_{\mathrm{DFT}} \tag{5}$$

where Λ is a tunable parameter and ΔE_{DFT} is the change in the DFT energy with respect to the minimum energy conformation. We chose the tunable parameter to be on the order

$\Lambda \sim 1\,\mu s^{-1} {E_h}^{-1}$.

We need to emphasize a couple of points regarding the objective function. First, Equation 2 attempts to describe a single conformer of definite geometry. There are theories that enable the inclusion of geometric relaxation (or reogranization)[38,39] and vibrational effects[40] in estimating the rates of RISC and fluorescence, and these would be the proper way to describe a dynamical ensemble of conformers.[41–43] However, the TADF rate maximization is a geometry optimization where we maximize the TADF rate instead of minimizing the energy, which necessitates the evaluation of the TADF rate at a definite geometry. Hence, consideration of nuclear dynamics is incompatible with the present investigation.

Second, Equation 2 represents an upper bound on the TADF rate. In the real universe, non-radiative decay and a finite RISC rate would entail a slowdown in addition to the fluorescence rate and the thermodynamic cap on the S_1 population. Nonetheless, the formula appeals to our purposes in a number of ways. In the first place, we are only interested in good TADF emitters, where TADF dominates over non-radiative decay, so it makes sense to compute the TADF rate by itself and verify after the fact that TADF proceeds on a feasible timescale. Moreover, Brédas *et al.* calculated the RISC rates of several TADF emitters and found that RISC rates on the microsecond timescale are not uncommon.[28] We expect that RISC would not be a severe bottleneck in most cases and that the formula would provide a tight upper bound on the TADF rate. Indeed, we found that the RISC only makes quantitative corrections and does not alter the qualitative trends in our model systems. The computational details and numerical results have been provided in the SI.

The electronic structure calculations were performed using the B3LYP exchange-correlation functional[44–49] and the 6-31+G* basis set[50–53] as implemented in the Q-Chem 5.1 software package.[54] The geometries were visualized in Avogadro 1.2.0,[55] and the natural transition orbitals (NTOs)[56] were visualized in MacMolPlt 7.7.[57] Standard hybrid functionals are known to underestimate the excitation energy and overestimate the CT character of CT-like states.[58,59] We are also neglecting the dielectric environment, which is known to stabilize

the CT-like states,[42] and the dielectric stabilization is not in principle equivalent to the CT error.[41] However, our objective was not to make quantitative predictions of TADF rates, but to extract qualitative trends that can guide the design of TADF emitters. Since analytical derivatives of the TDM are not available, the TADF rate maximization entails much higher computational costs than the usual energy minimization. Thus, it was desirable to use a functional that can reproduce the qualitative trends at minimal costs.

In order to establish that conformational dependence is not an artifact of B3LYP, the electronic structures at the key geometries were recalculated using PBE0,[60–62] M06-2X,[63] and LRC-ω^*PBE.[64–66] The asterisk indicates IPEA-tuning of the range-separation parameter, which we did at the minimum energy conformation in vacuum. Solvent effects were examined in the cases of M06-2X and LRC-ω^*PBE, using the integral equation formalism polarizable continuum model (IEF-PCM)[67–69] and first order, perturbative state-specific (ptSS)[70] treatment of the excited states. We used the dielectric constant and optical dielectric constant of toluene at room temperature: $\varepsilon = 2.379$ and $\varepsilon_\infty = 2.232$.[71]

The TADF rate maximization was performed using a variation of the Nelder-Mead simplex method.[72,73] Since there are multiple versions of the method, we have outlined our algorithm in the SI. The geometries of the molecules were represented in the Z-matrix coordinates. We have included the Z-matrices of the model systems at the key geometries in the SI. In order to reduce the computational costs and contain the geometric changes in the meaningful regions of the conformation space, a subset of the bond lengths, bond angles, and dihedral angles were chosen to be varied, while the others were constrained to the values at the minimum energy conformation. Since peripheral hydrogens should not have strong effects on the electronic structure and aromatic ring systems should be resistant to distortions, we chose the geometries of the single bonds that connect the aromatic ring systems as the variables. For a complete range of motion, six DOFs are required per bond: one bond length, two bond angles, and three dihedral angles. Hence, the number of variables in each of the model systems could be reduced to 30 or fewer Z-matrix coordinates. In order

to assess the extent to which our choices of variables were justified, a constrained energy minimization was performed at the end of the TADF rate maximization, where we relaxed the bond lengths and angles that had been fixed in the TADF rate maximization.

Results and Discussion

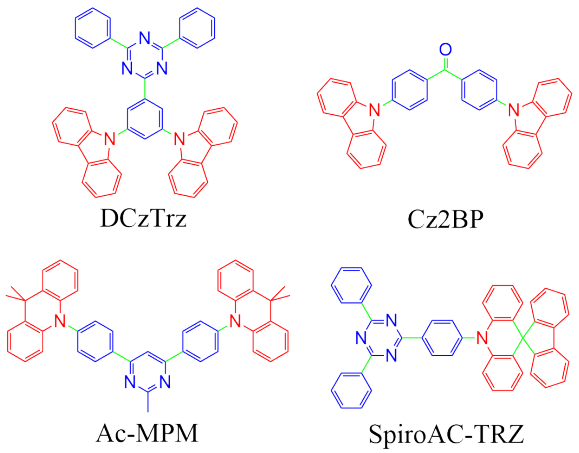

Figure 1: Skeletal structures of **DCzTrz**, **Cz2BP**, **Ac-MPM**, and **SpiroAC-TRZ**. The donor and acceptor groups are indicated in red and blue, respectively. Shown in green are the single bonds whose geometries were varied in the TADF rate maximization.

As model systems, we chose a number of TADF emitters that have been reported to exhibit high EQE in blue: **DCzTrz**,[23] **Cz2BP**,[74] **Ac-MPM**,[75] and **SpiroAC-TRZ**.[25] The skeletal structures of the model systems are shown in Figure 1. We are going to examine the case of **DCzTrz** in detail and use the other emitters to assess the extent to which the results can be generalized.

DCzTrz

Table 1 summarizes the energetics of **DCzTrz** at the maximum TADF geometries with various energy penalties. Between the energy minimum ($\Lambda = \infty$) and the TADF maximum with no energy penalty ($\Lambda = 0$), the TADF rate increases over two orders of magnitude from $9.4\,\mathrm{ms}^{-1}$ to $1.07\,\mu\mathrm{s}^{-1}$. Moreover, the enhancement is not a result of trade-off between

Table 1: Conformational energies, excitation energies, oscillator strengths, and TADF rates of **DCzTrz** at the maximum TADF geometries with various energy penalties. The case of $\Lambda = \infty$ corresponds to the energy minimum, and the case of $\Lambda = 0$ corresponds to the TADF maximum with no energy penalty.

Λ	ΔE_{DFT}	EE (eV)		k_{TADF}
($\mu s^{-1} {E_h}^{-1}$)	(kJ mol^{-1})	S_1 / T_1 / T_2	f_{10}	(μs^{-1})
∞	0	2.84 / 2.71 / 2.74	0.017	0.0094
8.0	211	2.86 / 2.83 / 2.93	0.026	0.88
4.0	278	2.94 / 2.91 / 3.00	0.029	1.06
2.0	409	2.86 / 2.84 / 2.95	0.026	1.08
0.0	594	2.79 / 2.77 / 2.90	0.028	1.07

a small ST gap and a large TDM: the S_1-T_1 gap decreases from 0.13 eV to 0.02 eV, and f_{10} increases from 0.017 to 0.028. The simultaneous improvement of what are supposed to be contraindicated properties confirms that conformational optimization has achieved more than modulation of the HOMO-LUMO overlap. Although the conformational energy also undergoes a gigantic increase of 594 kJ mol^{-1}, the results with energy penalty reveal that much of the energy is irrelevant to improving the TADF rate. Using $\Lambda = 4.0\,\mu s^{-1} {E_h}^{-1}$, the conformational energy can be halved with negligible loss in the TADF rate. Using $\Lambda = 8.0\,\mu s^{-1} {E_h}^{-1}$, further damping to 211 kJ mol^{-1} is possible with less than 20 % loss of the TADF rate enhancement. The stability of the TADF rate against an energy penalty affirms that the maximum TADF conformation is not an absurdity, but its essential features are ones that one may hope to reproduce using suitable techniques in the real universe.

Figure 2a shows the minimum energy conformation with arrows indicating the DOFs that participate in the TADF rate maximization. It is obvious that the TADF maximum in Figure 2b is a strained conformation. The carbazole (Cz, donor) groups have popped above and below the plane of the 2,4,6-triphenyl-1,3,5-triazine (Trz, acceptor) group by $-33.4°$ (left) and $+3.7°$ (right), respectively. To be precise, two of the phenyl rings have twisted with respect to the triazine ring, so the Trz group is no longer planar, so these angles are with respect to the phenyl ring that bridges the Cz groups to the rest of the Trz group. Also, the Cz groups have rotated to become more orthogonal to the Trz group. The Cz groups are

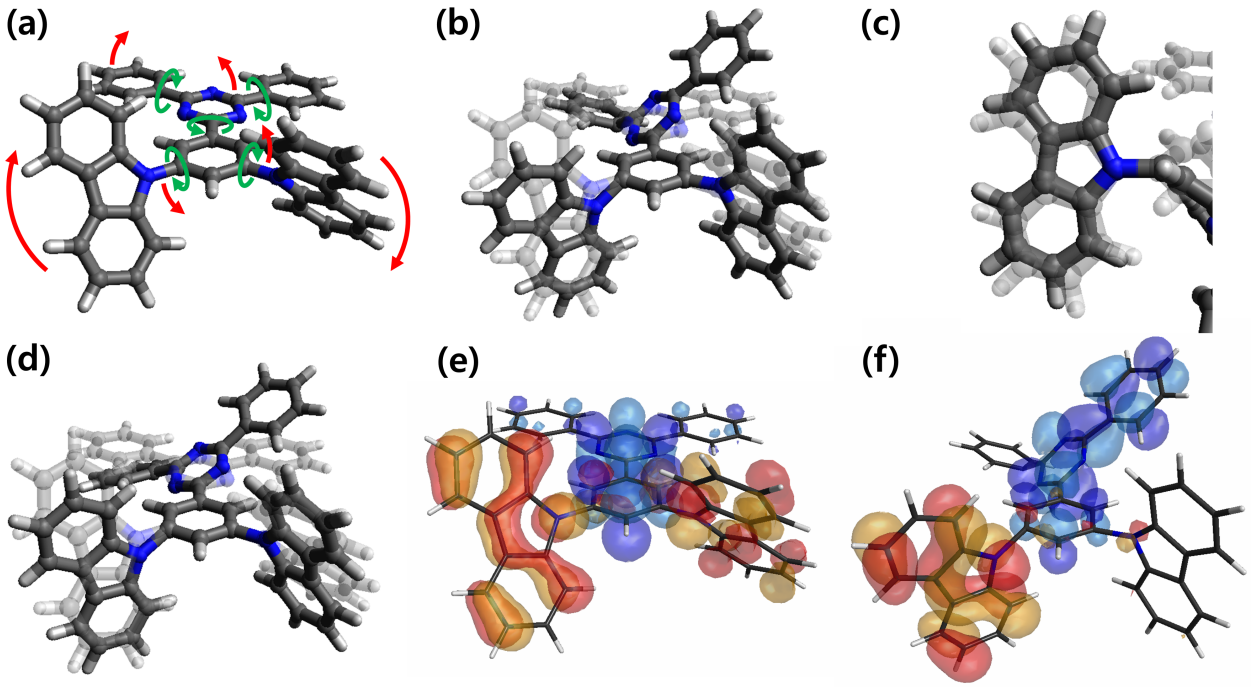

Figure 2: Geometries of **DCzTrz** at (a) the energy minimum ($\Lambda = \infty$); (b) the TADF maximum with no energy penalty ($\Lambda = 0$); (c) the donor-acceptor bond (maginfied view); and (d) the TADF maximum with energy penalty ($\Lambda = 8.0\,\mu s^{-1}{E_h}^{-1}$). Also, the dominant NTO pairs of the S_1 state at (e) the energy minimum ($\Lambda = \infty$) and (f) the TADF maximum with no energy penalty ($\Lambda = 0$). The arrows in (a) indicate the DOFs that are the most active in the TADF rate maximization, and the translucent geometries in the background of (b-d) are the minimum energy conformation. In (e-f), the hole orbitals are shown in red and orange, and the electron orbitals are shown in sky blue and indigo. Contour value: 0.025.

92.7° (left) and 79.8° (right) to the Trz group, respectively, in contrast to 57.3° (left) and 56.5° (right) at the energy minimum. Increasing the dihedral angle between the donor and acceptor moieties is a known strategy to reduce the HOMO-LUMO overlap and hence the ST gap.[76–78] The fact that the same motif appears at the TADF maximum of **DCzTrz** is an encouraging sign that useful design principles can be extracted.

Indeed, a strange feature comes to attention. After popping above and below the plane of the Trz group, the Cz groups tilt back towards the Trz group, as shown in Figure 2c. The lower and upper C_{Cz}-N_{Cz}-C_{Trz} angles at each Cz group differ by +17.7° (left) and −19.5° (right), respectively, whereas the C_{Cz}-N_{Cz}-C_{Trz} angles at the energy minimum are the same 125.7° ± 0.2°. Though the differences in the angles change to +23.8° (left) and −6.5° (right), the *gooseneck* persists even with an energy penalty of $\Lambda = 8.0\,\mu s^{-1} {E_h}^{-1}$. Hence, the gooseneck cannot be a side product of the optimization, but a feature relevant to TADF. Though the physical intuition is unclear, it might be associated with the additional terms in the four-state model[32] or the dissimilar forms of the integrands in the exchange integral $\langle {r_{12}}^{-1} \rangle$ and the transition dipole integral $\langle r_1 \rangle$. After all, the ST gap and the TDM should depend not only on the overlap, but also on the orientation of the HOMO and the LUMO.

Meanwhile, the twist in the Trz group tends to dissipate with energy penalty. As shown in Figure 2d, the phenyl rings return to a more coplanar arrangement to the triazine ring in what appears to be a concerted manner. However, the planarity of the Trz group remains quite disturbed even with an energy penalty of $\Lambda = 8.0\,\mu s^{-1} {E_h}^{-1}$. The phenyl rings to the front center and the back left are 30.2° and 30.6° to the triazine ring, respectively, which are 41.6° and 61.3° in the absence of energy penalty. We conjecture that the twist in the Trz group controls the distribution of the LUMO so that it gets neither too close to nor too far away from to the HOMO. Comparing the dominant NTO pairs of the S_1 state at the energy minimum (Figure 2e) and the TADF maximum (Figure 2f), the distribution of the S_1 hole is indeed impacted. The NTOs of the T_1 state are similar (Figure S4). This would

also explains why the twist appears to unroll in a concerted manner as energy penalties are imposed. Overall, the twist in the Trz group appears to help enhance the TADF rate, but a balance must be struck with the conformational energy.

Other Model Systems

Table 2: Conformational energies, excitation energies, oscillator strengths, and TADF rates of **Cz2BP**, **Ac-MPM**, and **SpiroAC-TRZ** at the maximum TADF geometries with various energy penalties. The case of $\Lambda = \infty$ corresponds to the energy minimum, and the case of $\Lambda = 0$ corresponds to the TADF maximum with no energy penalty.

	Λ ($\mu s^{-1} {E_h}^{-1}$)	ΔE_{DFT} (kJ mol^{-1})	EE (eV) S_1 / T_1 / T_2	f_{10}	k_{TADF} (μs^{-1})
Cz2BP	inf	0	2.99 / 2.67 / 2.78	0.345	1.9×10^{-4}
	8.0	162	2.67 / 2.63 / 2.64	0.061	0.66
	4.0	181	2.66 / 2.62 / 2.62	0.062	0.69
	0.0	193	2.64 / 2.60 / 2.61	0.060	0.69
Ac-MPM	inf	0	2.47 / 2.46 / 2.47	3.4×10^{-5}	0.0012
	8.0	51	2.51 / 2.49 / 2.49	0.036	0.59
	4.0	365	2.54 / 2.51 / 2.67	0.022	0.58
	0.0	420	2.55 / 2.52 / 2.61	0.028	0.63
SpiroAC-TRZ	inf	0	2.41 / 2.41 / 2.66	7.9×10^{-6}	4.2×10^{-4}
	8.0	104	2.56 / 2.54 / 2.75	0.012	0.49
	4.0	294	2.48 / 2.46 / 2.75	0.017	0.50
	0.0	475	2.50 / 2.48 / 2.67	0.019	0.61

Table 2 summarizes the energetics of **Cz2BP**, **Ac-MPM**, and **SpiroAC-TRZ**. The TADF rates start in the millisecond timescale at the energy minimum and end in the microsecond timescale at the TADF maximum, suggesting that TADF rate enhancements over two to three orders of magnitude might be typical in the conformational optimization of TADF emitters. **Cz2BP** undergoes the largest enhancement in the TADF rate, a factor of 3000. However, the improvement is a result of trade-off between a small ST gap and a large TDM: the S_1-T_1 gap and f_{10} both decrease from 0.32 eV to 0.04 eV and from 0.345 to 0.060, respectively. The cases of **Ac-MPM** and **SpiroAC-TRZ** might be more complicated. Whereas the increases in the S_1-T_1 gaps of 0.02 eV are comparable to the uncertainty, the increases in the f_{10} of **Ac-MPM** and **SpiroAC-TRZ** span three orders of magnitude

from 3.4×10^{-5} to 0.028 and from 7.9×10^{-6} to 0.019, respectively. The disproportionate trade-off suggests that conformational optimization might have had a non-trivial impact on the electronic structure. In any case, simultaneous improvement of the ST gap and the TDM might be a rare occurance, which might also explain why **DCzTrz** was the only model system whose TADF rate reached the submicrosecond regime.

Notice that the minimum energy conformations of **Ac-MPM** and **SpiroAC-TRZ** have a tiny ST gap. In particular, the ST gap of **SpiroAC-TRZ** is near vanishing. The two-state model would suggest that the SOC must vanish, since both the S_1 and T_1 states must be CT states.[27] Surprisingly, the RISC step does not appear to be the most severe bottleneck. The f_{10} and SOC are 7.9×10^{-6} and $0.0063\,\mathrm{cm}^{-1}$, respectively, which correspond to a fluorescence rate of $2.0\,\mathrm{ms}^{-1}$ and a RISC rate of $2.9\,\mathrm{ms}^{-1}$ (Table S1). This makes sense in light of the four-state model. The S_1 and T_1 states contain different fractions of the diabatic CT and LE states, and the electron exchange favors the S_1 state as the more CT-like state. Hence, the fluorescence step can end up slower than the RISC step. We refer interested readers to the work of de Silva *et al.*[32]

In each of the model systems, a suitable energy penalty can reduce the conformational energy with minimal loss in the TADF rate. Even with no energy penalty, the TADF maximum of **Cz2BP** has a conformational energy of $194\,\mathrm{kJ\,mol}^{-1}$, less than half of the other model systems. With an energy penalty of $\Lambda = 8.0\,\mu\mathrm{s}^{-1}{E_\mathrm{h}}^{-1}$, **Ac-MPM** and **SpiroAC-TRZ** reduce their conformational energies to $53\,\mathrm{kJ\,mol}^{-1}$ and $102\,\mathrm{kJ\,mol}^{-1}$, respectively, while retaining more than 90 % and 80 % of the TADF rates. Though these conformational energies might seem daunting, synthetic chemists have created and stabilized molecules with strain energies over $300\,\mathrm{kJ\,mol}^{-1}$.[79,80] For certain TADF emitters, the maximum TADF conformation might be synthesizable using suitable modifications in the real universe.

Figure 3 shows the geometries of **Cz2BP**, **Ac-MPM**, and **SpiroAC-TRZ** at the TADF maximum with no energy penalty ($\Lambda = 0$). The maximum TADF geometries with energy penalties and a detailed discussion of their relations to the energetics can be found in the

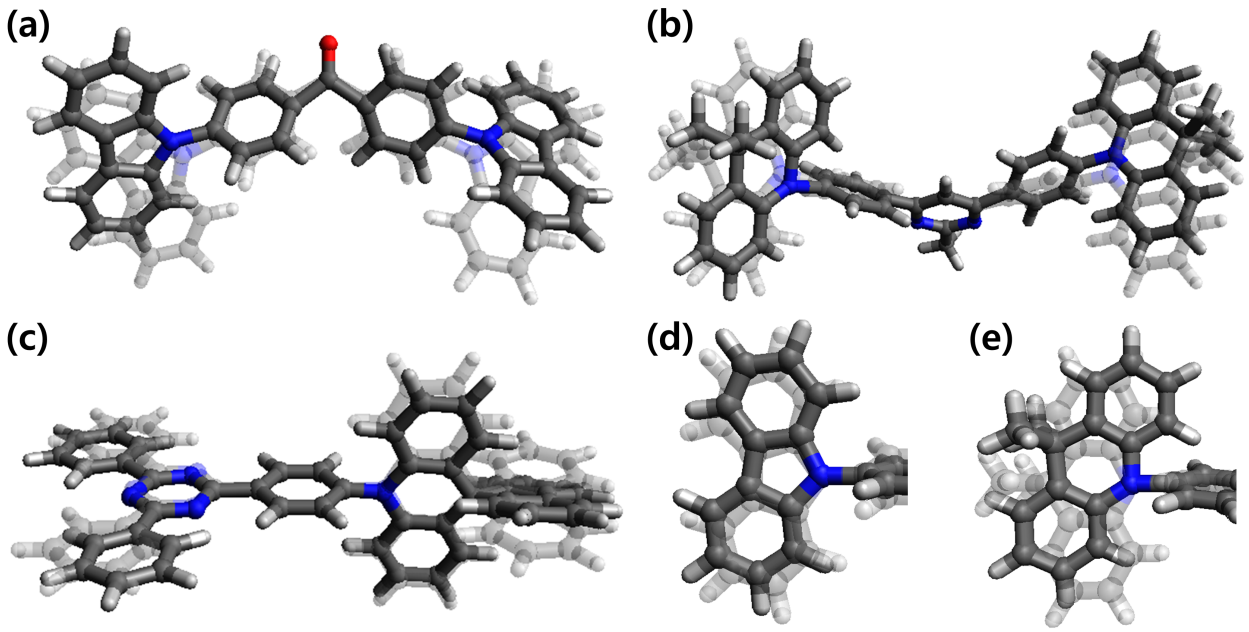

Figure 3: Geometries of (a) **Cz2BP**; (b) **Ac-MPM**; and (c) **SprioAC-TRZ** at the TADF maximum with no energy penalty ($\Lambda = 0$). Also, magnified views of the donor-acceptor bonds in (d) **Cz2BP** and (e) **Ac-MPM**. The translucent geometries in the background are the minimum energy conformations.

SI. Here, we summarize the key results. First, the dihedral angles between the donor and acceptor groups increase in **Cz2BP** (Figure 3a), while they decrease in **Ac-MPM** (Figure 3b) and **SpiroAC-TRZ** (Figure 3c). The dihedral angle changes are consistent with the outcome that the ST gap and the TDM both decrease in **Cz2BP** and increase in **Ac-MPM** and **SpiroAC-TRZ**. Second, **SpiroAC-TRZ** is the only model system that does not develop a gooseneck. The donor groups of **Cz2BP** (Figure 3d) and **Ac-MPM** (Figure 3e) both pop above and below the plane of the acceptor group and then tilt back towards the acceptor group. Third, the acceptor groups of **Cz2BP** and **Ac-MPM** become twisted, albeit in different ways from both **DCzTrz** and each other. In **Cz2BP**, the phenyl rings become more orthogonal to each other. In **Ac-MPM**, one of the phenyl rings twists out of plane, while the other maintains a moderate angle to the pyrimidine ring. The gooseneck and the twist in the acceptor group tend to persist even with energy penalties.

Remarkably, three out of the four model systems developed a gooseneck at the DA bond and a twist in the acceptor group. We suspect that these motifs might provide a useful

handle on the TADF rate in general DA systems. Unfortunately, there is want of theoretical intuition and experimental evidence at this point. Inspite of abundant efforts to manipulate the DA dihderal angles,[76–78] we are not aware of prior studies that have considered out-of-plane displacement of the donor and the acceptor moieties. As discussed earlier, the gooseneck might be associated with the mathematical forms of the integrals that enter the TADF rate, but it is unclear which integrals are affected in what way.

The twist in the acceptor group is also obscure. While it is not hard to rationalize how the twist might change the distribution of the LUMO, it is not always clear why a particular distribution should be more conducive to TADF than another, nor does there appear to be a pattern in how the acceptor groups become distorted. For example, **Ac-MPM** appears to push the LUMO towards just one of the donor groups, while **Cz2BP** remains much more symmetric. The dominant NTO pairs of the S_1 and T_1 states can be found in the SI. Perhaps, the absence of a trend is due to the small number of model systems. The twist might not be a single motif, but a collection of motifs that concern specific families of emitters.

On the other hand, the lack of physical intuition attests to the true value of conformational optimization: discovery of design principles that do not render themselves to deduction.

Choice of Density Functional

In order to assess the functional dependence of the results, we took the maximum TADF geometries optimized using B3LYP and recalculated the electronic structures using PBE0, M06-2X, and LRC-ω^*PBE. To our surprise, the generalized gradient approximation (GGA) global hybrid, the meta-GGA global hybrid, and the range-separated hybrid (RSH) exhibited similar patterns. Since tuned RSHs have been shown to be effective at predicting the excited state properties of TADF emitters,[41,81] we focus on LRC-ω^*PBE as the primary subject of comparison. The complete set of results can be found in the SI.

Table 3 summarizes the LRC-ω^*PBE energetics of **DCzTrz** at the B3LYP geometries.

Table 3: Conformational energies, excitation energies, oscillator strengths, and TADF rates of **DCzTrz** and **Ac-MPM** recomputed using LRC-ω^*PBE/IEF-PCM at the maximum TADF geometries optimized using B3LYP. The case of $\Lambda = \infty$ corresponds to the energy minimum, and the case of $\Lambda = 0$ corresponds to the TADF maximum with no energy penalty.

	Λ ($\mu s^{-1} {E_h}^{-1}$)	ΔE_{DFT} (kJ mol^{-1})	EE (eV) S$_1$ / T$_1$ / T$_2$	f_{10}	k_{TADF} (μs^{-1})
DCzTRZ (vacuum)	inf	0	3.39 / 3.07 / 3.14	0.0310	1.5×10^{-5}
	8.0	202	3.49 / 3.27 / 3.29	0.0133	2.8×10^{-4}
	4.0	267	3.49 / 3.26 / 3.27	0.0018	2.4×10^{-5}
	2.0	394	3.37 / 3.15 / 3.20	3.5×10^{-4}	7.1×10^{-6}
	0.0	573	3.33 / 2.93 / 3.11	3.9×10^{-4}	1.1×10^{-8}
DCzTRZ (toluene)	inf	0	3.30 / 3.07 / 3.08	0.0312	3.1×10^{-4}
	8.0	199	3.37 / 3.27 / 3.27	0.0146	0.024
	4.0	262	3.39 / 3.27 / 3.27	0.0021	0.0019
	2.0	389	3.28 / 3.14 / 3.21	4.2×10^{-4}	2.5×10^{-4}
	0.0	568	3.24 / 2.93 / 3.12	3.4×10^{-4}	2.7×10^{-7}
Ac-MPM (toluene)	inf	0	3.04 / 3.09 / 3.06	5.0×10^{-5}	0.0073
	8.0	48	2.97 / 2.98 / 3.07	0.031	3.8
	4.0	341	3.02 / 2.89 / 3.02	0.034	0.026
	0.0	393	3.08 / 2.82 / 3.08	0.0059	3.4×10^{-5}

Interestingly, the TADF rates in LRC-ω^*PBE seem to increase with the energy penalty at small values of Λ. The TADF rate reduces to $0.011\,s^{-1}$ at the greometry optimized with no energy penalty ($\Lambda = 0$), which is smaller than $15\,s^{-1}$ at the energy minimum. On the other hand, the maximum TADF rate is $280\,s^{-1}$ at the geometry optimized with $\Lambda = 8.0\,\mu s^{-1} {E_h}^{-1}$, which is an order of magnitude greater. A toluene-like environment stabilizes the S_1 state by 0.1 eV to 0.2 eV, increasing the maximum TADF rate to $24\,ms^{-1}$ at the geometry optimized with $\Lambda = 8.0\,\mu s^{-1} {E_h}^{-1}$, which is now two orders of magnitude greater than $0.31\,ms^{-1}$ at the energy minimum. The other molecules exhibit similar trends, as shown in Tables S4 and S6.

Remarkably, LRC-ω^*PBE predicts much more favorable TADF properties in **Ac-MPM** and **SpiroAC-TRZ**. Table 3 shows the energetics of **Ac-MPM** in a toluene-like environment as computed using LRC-ω^*PBE/IEF-PCM. Notice that **Ac-MPM** exhibits a simultaneous improvement of the ST gap and TDM and a TADF rate in the submicrosecond timescales at the geometry optimized with $\Lambda = 8.0\,\mu s^{-1} {E_h}^{-1}$. As shown in Table S6, **SpiroAC-TRZ** also exhibits a simultaneous improvement at $\Lambda = 4.0\,\mu s^{-1} {E_h}^{-1}$, though

the TADF rate is the greatest at $\Lambda = 8.0\,\mu s^{-1}{E_h}^{-1}$. The TADF rates of **Ac-MPM** and **SpiroAC-TRZ** are $3.8\,\mu s^{-1}$ and $2.9\,\mu s^{-1}$ at the respective geometries optimized with $\Lambda = 8.0\,\mu s^{-1}{E_h}^{-1}$. Again, we emphasize that we have not re-optimized the geometries using LRC-ω*PBE/IEF-PCM. It stands to reason that we could have gotten even more drastic enhancements if we had.

Hence, various functionals corroborate the enhancement of TADF rates in the B3LYP geometries, provided that the objective function contained sufficient energy penalty. We suspect that the TADF rate maximization had a propensity to exploit the quirks of the B3LYP universe and that the energy penalty helped the optimizer to remain in the safe region of the conformation space. The existence of such quirks is not surprising, since B3LYP is just an approximation to the exact density functional. However, B3LYP is not special in this regard. In fact, we might have encountered the same issue even if we had optimized the geometries using a different functional. Suppose that we had done the TADF rate maximization using LRC-ω*PBE/IEF-PCM. We would have obtained drastic enhancements, only to have those results be brought into question by the other functionals. For practical purposes, it would make sense to perform the TADF rate maximization using an inexpensive method and verify the improvements using more sophisticated methods.

We recapitulate the noteworthy commonalities in the energetics predicted by B3LYP and the other functionals. First, there exists a conformation where the TADF rate is orders of magnitude greater than at the minimum energy conformation. Moreover, the maximum TADF conformation in B3LYP and in the other functionals cannot be too far apart, considering that a moderate energy penalty is sufficient to arrive at a geometry that exhibits TADF rate enhancement in all of the functionals. These observations reaffirm that the maximum TADF conformation not only exists, but also can be determined to a reasonable precision. Second, one or more of the model systems exhibit a simultaneous improvement of the ST gap and TDM. These are **DCzTrz** in B3LYP and PBE0 and **Ac-MPM** and **SpiroAC-TRZ** in M06-2X/IEF-PCM and LRC-ω*PBE/IEF-PCM. When a simultaneous improvement of the

ST gap and TDM occurs, the maximium TADF rate can be impressive. The TADF rate of **DCzTrz** in B3LYP and the TADF rates of **Ac-MPM** and **SpiroAC-TRZ** in M06-2X/IEF-PCM and LRC-ω*PBE/IEF-PCM reach the submicrosecond timescales. It is possible but difficult to think that the simultaneous improvement is just a quirk in each of the functionals, given that the last two methods predicted simultaneous improvement in geometries optimized using a different functional. The results cast a serious doubt on the conventional wisdom that the trade-off is an inherent property of TADF emitters.

Choice of Conformational Variables

So far, we have assumed that the variables in the TADF rate maximization corresponded to the most flexible DOFs in the model systems. While the assumption does not affect the existence of conformations that maximize the TADF rate, it does affect the extent to which we can expect the maximum TADF conformation to be reproducible in the real universe. If our choice of conformational variables were appropriate, then the changes in the geometry and the consequent changes in the TADF rate would be minimal even if we relaxed the complementary DOFs. Hence, we took the maximum TADF geometries and performed a constrained energy minimization to relax the hydrogen atoms and the aromatic ring systems, which had been fixed in the TADF rate maximization.

Figure 4 summarizes the energetics of the maximum TADF geometries before and after the constrained energy minimization. The effects of the relaxation depend on the system. For example, **DCzTrz** undergoes an order-of-magnitude decrease in the TADF rate from $1.07\,\mu s^{-1}$ to $0.14\,\mu s^{-1}$, and a noticeable decrease in the DFT energy from $594\,kJ\,mol^{-1}$ to $472\,kJ\,mol^{-1}$, as shown in Figures 4a and Figure 4b, respectively. It appears that our choice of variables included too many rigid DOFs, or the geometric changes might have been severe enough to obscure the distinction of flexible and rigid DOFs. Figure 2c reveals that the constrained energy minimization causes distortions in the phenyl and the triazine rings that tend to restore the planarity of the Trz group. These changes agree with the conjecture that

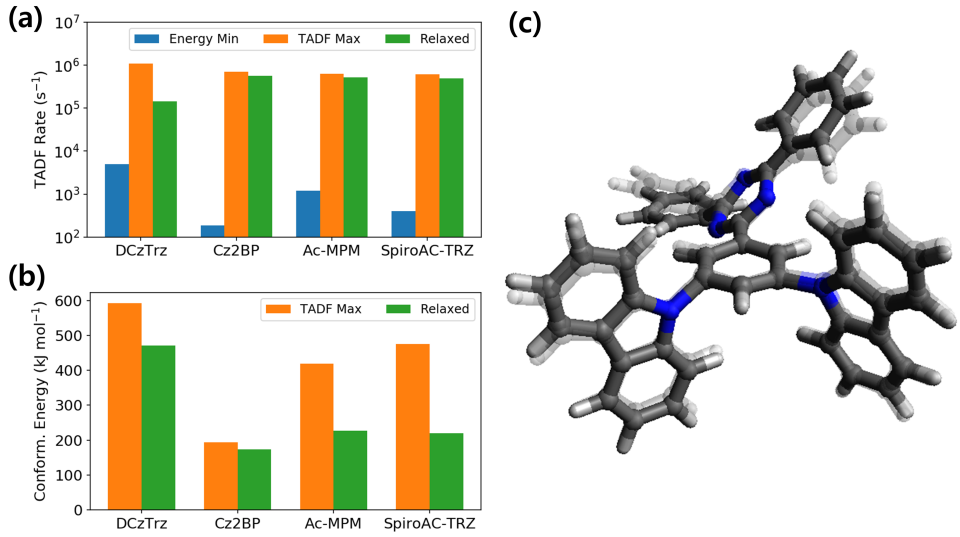

Figure 4: (a) TADF rates and (b) DFT energies of **DCzTrz**, **Cz2BP**, **Ac-MPM**, and **SprioAC-TRZ** at the energy minimum, at the TADF maximum ($\Lambda = 0$), and after the relaxation of the hydrogen atoms and the aromatic ring systems. (c) Geometry of **DCzTrz** at the TADF maximum ($\Lambda = 0$) after the relaxation of the hydrogen atoms and the aromatic ring systems.

the twist in the acceptor group imparts a considerable strain on **DCzTrz**. Also, it makes sense that unrolling the twist in the acceptor group in an unconcerted manner would be detrimental to the TADF rate, since the distortion controls the distribution of the LUMO.

With the exception of **DCzTrz**, the TADF rate enhancement is quite stable against the relaxation of the hydrogen atoms and the aromatic ring systems. **Cz2BP** shows minimal changes in both the TADF rate and the DFT energy, meaning that our choice of variables captured both the most flexible DOFs and the DOFs that are the most relevant to the TADF rate. In the cases of **Ac-MPM** and **SprioAC-TRZ**, the conformational energies are halved, but the TADF rates remain at $0.52\,\mu s^{-1}$ and $0.49\,\mu s^{-1}$, respectively. The geometries of **Cz2BP**, **Ac-MPM**, and **SprioAC-TRZ** after the constrained energy minimization have been provided in the SI. In addition to affirming our choice of variables, the stability of the TADF rate suggests a substantial overlap between the most flexible DOFs and the DOFs that determine the TADF rate in the model systems. The outcome is consistent with our proposition that the essential features of the maximum TADF conformation might be

synthesizable using suitable modifications in the real universe.

How to synthesize the maximum TADF conformers is beyond the scope of this work, but we can suggest some basic examples. The textbook chemist's approach would be to attach bulky groups that constrain the rotation of certain bonds – the same approach has been used to modulate the donor-acceptor dihedral angles in TADF emitters.[76–78] We can also imagine placing the organic layer under mechanical stress or pressure to crowd the molecules together. In the first place, it is not necessary to have every OLED molecule in the maximum TADF conformation. For most practical purposes, it would suffice to increase the population of molecules that have higher TADF rate than the equilibrium ensemble of the original emitter. We expect that a myriad of techniques in enzyme design might prove applicable to the conformational engineering of TADF OLEDs.

Conclusions

In order to demonstrate the potential of conformational optimization to assist the development of trend-breaking TADF OLEDs, we studied direct maximization of the TADF rate in the conformation spaces of several TADF emitters. As desired, one of the model systems achieved a simultaneous improvement of the ST gap and the TDM, and its simulated TADF rate could be brought into the submicrosecond timescales (**DCzTrz**). Even model systems that exhibited trade-off between a small ST gap and a large TDM were found to undergo TADF rate enhancements by two to three orders of magnitude. The conformational energy required to maximize the TADF rate can be as small as $193\,\mathrm{kJ\,mol^{-1}}$ even in the absence of energy penalty (**Cz2BP**), and the conformational energy can be as small as $51\,\mathrm{kJ\,mol^{-1}}$ with minimal loss in the TADF rate enhancement (**Ac-MPM**). Furthermore, the maximum TADF conformations of the model systems shared a number of structural motifs, such as the gooseneck at the DA bond and the concerted rotation of the aromatic rings in the acceptor group. Although the physical intuition behind these motifs remain obscure, the opacity itself

demonstrates the true value of conformational optimization: discovery of design principles that do not render themselves to deduction.

The conformational dependence of the TADF rate motivates the incorporation of conformational engineering into the TADF technology. Based on the results of TADF rate maximization with energy penalties and constrained energy minimization, the maximum TADF conformation of certain molecules, or another conformation that contains its essential features, might be synthesizable, given the high levels of strain that are within the reach of modern synthetic chemistry. Since the minimum energy conformation is not the best geometry in terms of the TADF rate, it would be desirable to manipulate the conformation in a way that enhances the TADF rate. Although the proposition might seem unorthodox in physical or organic chemistry, changing the properties of a molecule by changing its conformation is a standard in fields such as enzyme design. In the future, we hope to connect conformational optimization with experimental efforts and demonstrate that the electronic structures of TADF emitters can be improved in the real universe.

Acknowledgement

This work was supported by a grant from the U.S. Department of Energy Office of Basic Energy Sciences (DE-FG02-07ER46474).

Supporting Information Available

Our version of the Nelder-Mead simplex method; calculation of the RISC rate and evaluation of its effects on the TADF rate; recalculation of the electronic structures using PBE0, M06-2X, LRC-ω*PBE, M06-2X/IEF-PCM and LRC-ω*PBE/IEF-PCM; geometries of **Cz2BP**, **Ac-MPM**, and **SprioAC-TRZ** at the TADF maximum with various energy penalties, and after the relaxation of DOFs that had been fixed in the TADF rate maximization; dominant NTO pairs of **DCzTrz**, **Cz2BP**, **Ac-MPM**, and **SprioAC-TRZ** in the S_1 and T_1 states;

Z-matrices thereof.

References

(1) Tang, C. W.; VanSlyke, S. A. Organic electroluminescent diodes. *Appl. Phys. Lett.* **1987**, *51*, 913–915.

(2) Burrows, P. E.; Gu, G.; Bulovic, V.; Shen, Z.; Forrest, S. R.; Thompson, M. E. Achieving full-color organic light-emitting devices for lightweight, flat-panel displays. *IEEE Trans. Electron Devices* **1997**, *44*, 1188–1203.

(3) Geffroy, B.; le Roy, P.; Prat, C. Organic light-emitting diode (OLED) technology: materials, devices and display technologies. *Polym. Int.* **2006**, *55*, 572–582.

(4) Xiao, L.; Chen, Z.; Qu, B.; Luo, J.; Kong, S.; Gong, Q.; Kido, J. Recent Progresses on Materials for Electrophosphorescent Organic Light-Emitting Devices. *Adv. Mater.* **2011**, *23*, 926–952.

(5) de Almeida, A.; Zissis, G.; Quicheron, M.; Bertldi, P. *Accelerating the Deployment of Solid State Lighting (SSL) in Europe*; EUR 25596 EN; European Commission Joint Research Centre: Ispra (VA), Italy, 2012.

(6) Penning, J.; Stober, K.; Taylor, V.; Yamada, M. *Energy Savings Forecast of Solid-State Lighting in General Illumination Applications*; DOE/EE-1467; U.S. Department of Energy Office of Energy Efficiency and Renewable Energy: Washington D.C., 2016.

(7) Sasabe, H.; Kido, J. Recent Progress in Phosphorescent Organic Light-Emitting Devices. *Eur. J. Org. Chem.* **2013**, *34*, 7653–7663.

(8) Wong, M. Y.; Zysman-Colman, E. Purely Organic Thermally Activated Delayed Fluorescence Materials for Organic LightEmitting Diodes. *Adv. Mater.* **2017**, *29*, 1605444.

(9) Baldo, M. A.; O'Brien, D. F.; You, Y.; Shoustikov, A.; Sibley, S.; Thompson, M. E.; Forrest, S. R. Highly efficient phosphorescent emission from organic electroluminescent devices. *Nature* **1998**, *395*, 151–154.

(10) Minaev, B.; Baryshnikov, G.; Agren, H. Principles of phosphorescent organic light emitting devices. *Phys. Chem. Chem. Phys.* **2014**, *16*, 1719–1758.

(11) Zhang, Y.; Lee, J.; Forrest, S. R. Tenfold increase in the lifetime of blue phosphorescent organic light-emitting diodes. *Nat. Commun.* **2014**, *5*, 1–7.

(12) Parker, C. A.; Hatchard, C. G. Triplet-singlet emission in fluid solutions. Phosphorescence of eosin. *Trans. Faraday Soc.* **1961**, *57*, 1894–1904.

(13) Endo, A.; Ogasawara, M.; Takahashi, A.; Yokoyama, D.; Kato, Y.; Adachi, C. Thermally Activated Delayed Fluorescence from Sn^{4+}–Porphyrin Complexes and Their Application to Organic Light Emitting Diodes – A Novel Mechanism for Electroluminescence. *Adv. Mater.* **2009**, *21*, 4802–4806.

(14) Endo, A.; Sato, K.; Yoshimura, K.; Kai, T.; Kawada, A.; Miyazaki, H.; Adachi, C. Efficient up-conversion of triplet excitons into a singlet state and its application for organic light emitting diodes. *Appl. Phys. Lett.* **2011**, *98*, 083302.

(15) Uoyama, H.; Goushi, K.; Shizu, K.; Nomura, H.; Adachi, C. Highly efficient organic light-emitting diodes from delayed fluorescence. *Nature* **2012**, *492*, 234–238.

(16) Lee, J.; Shizu, K.; Tanaka, H.; Nomura, H.; Yasuda, T.; Adachi, C. Oxadiazole-and triazole-based highly-efficient thermally activated delayed fluorescence emitters for organic light-emitting diodes. *J. Mater. Chem. C* **2013**, *1*, 4599–4604.

(17) Kawasumi, K.; Wu, T.; Zhu, T.; Chae, H. S.; Van Voorhis, T.; Baldo, M. A.; Swager, T. M. Thermally Activated Delayed Fluorescence Materials Based on Homocon-

jugation Effect of Donor–Acceptor Triptycenes. *J. Am. Chem. Soc.* **2015**, *137*, 11908–11911.

(18) Liu, Y.; Xie, G.; Wu, K.; Luo, Z.; Zhou, T.; Zeng, X.; Yu, J.; Gong, S.; Yang, C. Boosting reverse intersystem crossing by increasing donors in triarylboron/phenoxazine hybrids: TADF emitters for high-performance solution-processed OLEDs. *J. Mater. Chem. C* **2016**, *4*, 4402–4407.

(19) Nobuyasu, R. S.; Ren, Z.; Griffiths, G. C.; Batsanov, A. S.; Data, P.; Yan, S.; Monkman, A. P.; Bryce, M. R.; Dias, F. B. Rational Design of TADF Polymers Using a Donor–Acceptor Monomer with Enhanced TADF Efficiency Induced by the Energy Alignment of Charge Transfer and Local Triplet Excited States. *Adv. Opt. Mater.* **2016**, *4*, 597–607.

(20) Sarma, M.; Wong, K.-T. Exciplex: An Intermolecular Charge-Transfer Approach for TADF. *ACS Appl. Mater. Interfaces* **2018**, *10*, 19279–19304.

(21) Shu, Y.; Levine, B. G. Simulated evolution of fluorophores for light emitting diodes. *J. Chem. Phys.* **2015**, *142*, 104104.

(22) Gómez-Bombarelli, R.; Aguilera-Iparraguirre, J.; Hirzel, T. D.; Duvenaud, D.; Maclaurin, D.; Blood-Forsythe, M. A.; Chae, H. S.; Einzinger, M.; Ha, D.-G.; Wu, T. et al. Design of efficient molecular organic light-emitting diodes by a high-throughput virtual screening and experimental approach. *Nat. Mater.* **2016**, *15*, 1120–1127.

(23) Kim, M.; Jeon, S. K.; Hwang, S.-H.; Lee, J. Y. Stable Blue Thermally Activated Delayed Fluorescent Organic LightEmitting Diodes with Three Times Longer Lifetime than Phosphorescent Organic LightEmitting Diodes. *Adv. Mater.* **2015**, *27*, 2515–2520.

(24) dos Santos, P. L.; Ward, J. S.; Bryce, M. R.; Monkman, A. P. Using Guest–Host Interactions To Optimize the Efficiency of TADF OLEDs. *J. Phys. Chem. Lett.* **2016**, *7*, 3341–3346.

(25) Lin, T.-A.; Chatterjee, T.; Tsai, W.-L.; Lee, W.-K.; Wu, M.-J.; Jiao, M.; Pan, K.-C.; Yi, C.-L.; Chung, C.-L.; Wong, K.-T. et al. Sky-Blue Organic Light Emitting Diode with 37% External Quantum Efficiency Using Thermally Activated Delayed Fluorescence from Spiroacridine-Triazine Hybrid. *Adv. Mater.* **2016**, *28*, 6976–6983.

(26) Cui, L.-S.; Nomura, H.; Geng, Y.; Kim, J. U.; Nakanotani, H.; Adachi, C. Controlling Singlet–Triplet Energy Splitting for Deep-Blue Thermally Activated Delayed Fluorescence Emitters. *Angew. Chem. Int. Ed.* **2017**, *56*, 1571–1575.

(27) El-Sayed, M. SpinOrbit Coupling and the Radiationless Processes in Nitrogen Heterocyclics. *J. Chem. Phys.* **1963**, *38*, 2834–2838.

(28) Samanta, P. K.; Kim, D.; Coropceanu, V.; Brédas, J.-L. Up-Conversion Intersystem Crossing Rates in Organic Emitters for Thermally Activated Delayed Fluorescence: Impact of the Nature of Singlet vs Triplet Excited States. *J. Am. Chem. Soc.* **2017**, *139*, 4042–4051.

(29) Tu, Z.; Han, G.; Hu, T.; Duan, R.; Yi, Y. Nature of the Lowest Singlet and Triplet Excited States of Organic Thermally Activated Delayed Fluorescence Emitters: A Self-Consistent Quantum Mechanics/Embedded Charge Study. *Chem. Mater.* **2019**, *31*, 6665–6671.

(30) Etherington, M. K.; Gibson, J.; Higginbotham, H. F.; Penfold, T. J.; Monkman, A. P. Revealing the spin–vibronic coupling mechanism of thermally activated delayed fluorescence. *Nat. Commun.* **2016**, *7*, 13680.

(31) Gibson, J.; Monkman, A. P.; Penfold, T. J. The Importance of Vibronic Coupling for Efficient Reverse Intersystem Crossing in Thermally Activated Delayed Fluorescence Molecules. *ChemPhysChem* **2016**, *17*, 2956–2961.

(32) de Silva, P.; Kim, C. A.; Zhu, T.; Van Voorhis, T. Extracting Design Principles for

Efficient Thermally Activated Delayed Fluorescence (TADF) from a Simple Four-State Model. *Chem. Mater.* **2019**, *31*, 6995–7006.

(33) Northey, T.; Stacey, J.; Penfold, T. J. The role of solid state solvation on the charge transfer state of a thermally activated delayed fluorescence emitter. *J. Mater. Chem. C* **2017**, *5*, 11001–11009.

(34) Evans, E. W.; Olivier, Y.; Puttisong, Y.; Myers, W. K.; Hele, T. J. H.; Menke, S. M.; Thomas, T. H.; Credgington, D.; Beljonne, D.; Friend, R. H. et al. Vibrationally Assisted Intersystem Crossing in Benchmark Thermally Activated Delayed Fluorescence Molecules. *J. Phys. Chem. Lett.* **2018**, *9*, 4053–4058.

(35) Hu, T.; Han, G.; Tu, Z.; Duan, R.; Yi, Y. Origin of High Efficiencies for Thermally Activated Delayed Fluorescence Organic Light-Emitting Diodes: Atomistic Insight into Molecular Orientation and Torsional Disorder. *J. Phys. Chem. C* **2018**, *122*, 27191–27197.

(36) Zhang, Q.; Li, B.; Huang, S.; Nomura, H.; Tanaka, H.; Adachi, C. Efficient blue organic light-emitting diodes employing thermally activated delayed fluorescence. *Nat. Photonics* **2014**, *8*, 326–332.

(37) Hilborn, R. C. Einstein coefficients, cross sections, f values, dipole moments, and all that. *Am. J. Phys.* **1982**, *50*, 982–986.

(38) Marcus, R. A. On the Theory of Oxidation-Reduction Reactions Involving Electron Transfer. I. *J. Chem. Phys.* **1956**, *24*, 966–978.

(39) Marcus, R. A. Chemical and Electrochemical Electron-Transfer Theory. *Annu. Rev. Phys. Chem.* **1964**, *15*, 155–196.

(40) Jortner, J. Temperature dependent activation energy for electron transfer between biological molecules. *J. Chem. Phys.* **1976**, *64*, 4860–4867.

(41) Sun, H.; Zhong, C.; Brdas, J.-L. Reliable Prediction with Tuned Range-Separated Functionals of the SingletTriplet Gap in Organic Emitters for Thermally Activated Delayed Fluorescence. *J. Chem. Theory Comput.* **2015**, *11*, 3851–3858.

(42) Mewes, J.-M. Modeling TADF in organic emitters requires a careful consideration of the environment and going beyond the FranckCondon approximation. *Phys. Chem. Chem. Phys.* **2018**, *20*, 12454–12469.

(43) Saigo, M.; Miyata, K.; Tanaka, S.; Nakanotani, H.; Adachi, C.; Onda, K. Suppression of Structural Change upon S1T1 Conversion Assists the Thermally Activated Delayed Fluorescence Process in Carbazole-Benzonitrile Derivatives. *J. Phys. Chem. Lett.* **2019**, *10*, 2475–2480.

(44) Vosko, S. H.; Wilk, L.; Nusair, M. Accurate spin-dependent electron liquid correlation energies for local spin density calculations: a critical analysis. *Can. J. Phys.* **1980**, *58*, 1200–1211.

(45) Becke, A. D. Density-functional exchange-energy approximation with correct asymptotic behavior. *Phys. Rev. A* **1988**, *38*, 3098–3100.

(46) Lee, C.; Yang, W.; Parr, R. G. Development of the Colle-Salvetti correlation-energy formula into a functional of the electron density. *Phys. Rev. B* **1988**, *37*, 785–789.

(47) Becke, A. D. Density-functional thermochemistry. III. The role of exact exchange. *J. Chem. Phys.* **1993**, *98*, 5648–5652.

(48) Stephens, P. J.; Devlin, F. J.; Chabalowski, C. F.; Frisch, M. J. Ab Initio Calculation of Vibrational Absorption and Circular Dichroism Spectra Using Density Functional Force Fields. *J. Phys. Chem.* **1994**, *98*, 11623–11627.

(49) Kim, K.; Jordan, K. D. Comparison of Density Functional and MP2 Calculations on the Water Monomer and Dimer. *J. Phys. Chem.* **1994**, *98*, 10089–10094.

(50) Hariharan, P. C.; Pople, J. A. The influence of polarization functions on molecular orbital hydrogenation energies. *Theor. Chim. Acta* **1973**, *28*, 213–222.

(51) Krishnan, R.; Binkley, J. S.; Seeger, R.; Pople, J. A. Self-consistent molecular orbital methods. XX. A basis set for correlated wave functions. *J. Chem. Phys.* **1980**, *72*, 650–654.

(52) Francl, M. M.; Pietro, W. J.; Hehre, W. J.; Binkley, J. S.; Gordon, M. S.; DeFrees, D. J.; Pople, J. A. Self-consistent molecular orbital methods. XXIII. A polarization-type basis set for second-row elements. *J. Chem. Phys.* **1982**, *77*, 3654–3665.

(53) Clark, T.; Chandrasekhar, J.; Spitznagel, G. W.; Schleyer, P. V. R. Efficient diffuse function-augmented basis sets for anion calculations. III. The 3-21+G basis set for first-row elements, Li–F. *J. Comput. Chem.* **1983**, *4*, 294–301.

(54) Shao, Y.; Gan, Z.; Epifanovsky, E.; Gilbert, A. T. B.; Wormit, M.; Kussmann, J.; Lange, A. W.; Behn, A.; Deng, J.; Feng, X. et al. Advances in molecular quantum chemistry contained in the Q-Chem 4 program package. *Mol. Phys.* **2015**, *113*, 184–215.

(55) Hanwell, M. D.; Curtis, D. E.; Lonie, D. C.; Vandermeersch, T.; Zurek, E.; Hutchison, G. R. Avogadro: an advanced semantic chemical editor, visualization, and analysis platform. *J. Cheminformatics* **2012**, *4*, 17.

(56) Martin, R. L. Natural transition orbitals. *J. Chem. Phys.* **2003**, *118*, 4775–4777.

(57) Bode, B. M.; Gordon, M. S. MacMolPlt: a graphical user interface for GAMESS. *J. Mol. Graph. Model.* **1998**, *16*, 133–138.

(58) Dreuw, A.; Head-Gordon, M. Failure of Time-Dependent Density Functional Theory for Long-Range Charge-Transfer Excited States: The Zincbacteriochlorin–Bacteriochlorin

and Bacteriochlorophyll–Spheroidene Complexes. *J. Am. Chem. Soc.* **2004**, *126*, 4007–4016.

(59) Dreuw, A.; Head-Gordon, M. Single-Reference ab Initio Methods for the Calculation of Excited States of Large Molecules. *Chem. Rev.* **2005**, *105*, 4009–4037.

(60) Perdew, J. P.; Burke, K.; Ernzerhof, M. Generalized Gradient Approximation Made Simple. *Phys. Rev. Lett.* **1996**, *77*, 3865–3868.

(61) Perdew, J. P.; Ernzerhof, M.; Burke, K. Rationale for mixing exact exchange with density functional approximations. *J. Chem. Phys.* **1996**, *105*, 9982–9985.

(62) Adamo, C.; Barone, V. Toward reliable density functional methods without adjustable parameters: The PBE0 model. *J. Chem. Phys.* **1999**, *110*, 6158–6170.

(63) Zhao, Y.; Truhlar, D. G. The M06 suite of density functionals for main group thermochemistry, thermochemical kinetics, noncovalent interactions, excited states, and transition elements: two new functionals and systematic testing of four M06-class functionals and 12 other functionals. *Theor. Chem. Acc.* **2008**, *120*, 215–241.

(64) Rohrdanz, M. A.; Herbert, J. M. Simultaneous benchmarking of ground- and excited-state properties with long-range-corrected density functional theory. *J. Chem. Phys.* **2008**, *129*, 034107.

(65) Henderson, T. M.; Janesko, B. G.; Scuseria, G. E. Generalized gradient approximation model exchange holes for range-separated hybrids. *J. Chem. Phys.* **2008**, *128*, 194105.

(66) Salzner, U.; Baer, R. Koopmans springs to life. *J. Chem. Phys* **2009**, *131*, 231101.

(67) Cancs, E.; Mennucci, B.; Tomasi, J. A new integral equation formalism for the polarizable continuum model: Theoretical background and applications to isotropic and anisotropic dielectrics. *J. Chem. Phys.* **1997**, *107*, 3032–3041.

(68) Chipman, D. M. Reaction field treatment of charge penetration. *J. Chem. Phys.* **2000**, *112*, 5558–5565.

(69) Cancs, E.; Mennucci, B. Comment on Reaction field treatment of charge penetration [J. Chem. Phys. 112, 5558 (2000)]. *J. Chem. Phys.* **2001**, *114*, 4744–4745.

(70) Mewes, J.-M.; You, Z.-Q.; Wormit, M.; Kriesche, T.; Herbert, J. M.; Dreuw, A. Experimental Benchmark Data and Systematic Evaluation of Two a Posteriori, Polarizable-Continuum Corrections for Vertical Excitation Energies in Solution. *The Journal of Physical Chemistry A* **2015**, *119*, 5446–5464.

(71) Marchal, J.; Lapp, C. Dielectric properties of polymethyl methacrylate in dilute solution previous results. *J. Polym. Sci.* **1958**, *27*, 571–573.

(72) Spendley, W.; Hext, G. R.; Himsworth, F. R. Sequential Application of Simplex Designs in Optimisation and Evolutionary Operation. *Technometrics* **1962**, *4*, 441–461.

(73) Nelder, J. A.; Mead, R. A Simplex Method for Function Minimization. *Comput. J.* **1965**, *7*, 308–313.

(74) Lee, S. Y.; Yasuda, T.; Yang, Y. S.; Zhang, Q.; Adachi, C. Luminous Butterflies: Efficient Exciton Harvesting by Benzophenone Derivatives for Full-Color Delayed Fluorescence OLEDs. *Angew. Chem. Int. Ed.* **2014**, *53*, 6402–6406.

(75) Komatsu, R.; Sasabe, H.; Seino, Y.; Nakao, K.; Kido, J. Light-blue thermally activated delayed fluorescent emitters realizing a high external quantum efficiency of 25% and unprecedented low drive voltages in OLEDs. *J. Mater. Chem. C* **2016**, *4*, 2274–2278.

(76) Huang, W.; Einzinger, M.; Zhu, T.; Chae, H. S.; Jeon, S.; Ihn, S.-G.; Sim, M.; Kim, S.; Su, M.; Teverovskiy, G. et al. Molecular Design of Deep Blue Thermally Activated Delayed Fluorescence Materials Employing a Homoconjugative Triptycene Scaffold and Dihedral Angle Tuning. *Chem. Mater.* **2018**, *30*, 1462–1466.

(77) Huang, W.; Einzinger, M.; Maurano, A.; Zhu, T.; Tiepelt, J.; Yu, C.; Chae, H. S.; Van Voorhis, T.; Baldo, M. A.; Buchwald, S. L. Large Increase in External Quantum Efficiency by Dihedral Angle Tuning in a Sky-Blue Thermally Activated Delayed Fluorescence Emitter. *Adv. Opt. Mater.* **2019**, *7*, 1900476.

(78) Zhan, L.; Xiang, Y.; Chen, Z.; Wu, K.; Gong, S.; Xie, G.; Yang, C. Fine-tuning the photophysical properties of thermally activated delayed fluorescent emitters using torsion angles: high performance sky-blue OLEDs. *J. Mater. Chem. C* **2019**, *7*, 13953–13959.

(79) Ohlendorf, G.; Mahler, C. W.; Jester, S.-S.; Schnakenburg, G.; Grimme, S.; Hger, S. Highly Strained Phenylene Bicyclophanes. *Angew. Chem. Int. Edit.* **2013**, *52*, 12086–12090.

(80) Liu, Y.-Y.; Lin, J.-Y.; Bo, Y.-F.; Xie, L.-H.; Yi, M.-D.; Zhang, X.-W.; Zhang, H.-M.; Loh, T.-P.; Huang, W. Synthesis and Crystal Structure of Highly Strained [4]Cyclofluorene: Green-Emitting Fluorophore. *Org. Lett.* **2016**, *18*, 172–175.

(81) Penfold, T. J. On Predicting the Excited-State Properties of Thermally Activated Delayed Fluorescence Emitters. *J. Phys. Chem. C* **2015**, *119*, 13535–13544.

TOC Graphic

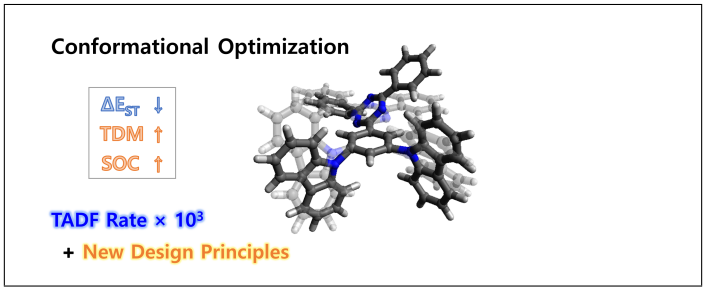
Conformational Optimization
ΔE_ST ↓
TDM ↑
SOC ↑
TADF Rate × 10³
+ New Design Principles